

Interfacial Chemistry on Carboxylate-Functionalized Monolayer Assemblies

OLGA GERSHEVITZ, ALINA OSNIS, AND CHAIM N. SUKENIK*
Department of Chemistry, Bar-Ilan University, Ramat Gan 52900, Israel

(Received 18 February 2005)

Abstract. Deposition of trichlorosilanes with ester groups at their remote termini provides a convenient entry to carboxylic acid-bearing siloxane-anchored self-assembled monolayers. The de-esterification of these esters has been optimized to minimize monolayer damage, and their quantitative re-esterification provides clear evidence for the stability of these systems. Both the structure of the ester-terminated monolayer and its de-esterification/esterification chemistry can be easily monitored by FTIR-ATR measurements. This spectroscopic tool, together with a liquid cell that enables IR spectra to be measured in an aqueous environment, enables a detailed structural analysis of the carboxylic acid-bearing siloxane-anchored self-assembled monolayers and an assessment of their acid/base behavior (by in situ titration). The use of D₂O instead of H₂O for the in situ titration experiments also improves the available IR window. Both monomeric and dimeric/oligomeric acid groups are seen, and the relative ease of deprotonation of these various species can be directly monitored. Monomers of alkyl carboxylic acids that are hydrogen bonded only to surrounding water molecules have a $pK_a = 4.9$, while the pK_a for the aggregated molecules is 9.3. Similar behavior is seen for surface-bound benzoic acids, where the two pK_a values are 4.7 and 9.0. The influence of temperature on these structures and their chemistry has been explored to a limited extent as well. When the alkylcarboxylic acid system is cooled to 10 °C, the pK_a value for the acid monomers is reduced from 4.9 to 4.5 and increases from 9.3 to 10.3 for the aggregates.

INTRODUCTION

Intermolecular forces at surfaces on the micro- and nanometer scale are central to a wide range of biological, chemical, and physical processes (e.g., heterogeneous catalysis, colloidal chemistry, adhesives, lubrication, membrane transport, molecular recognition, cell signaling, and control of a range of biochemical processes).¹⁻⁷ Interactions that play a major role in controlling these phenomena include van der Waals forces, hydrogen bonding, and electrostatic charge interactions.⁸

The acid/base properties of surface-confined molecular species are of fundamental and practical interest in a variety of diverse chemical phenomena.⁹⁻¹⁴ It is generally understood that the effective pK_a of a surface-immobilized molecule may be significantly different than that of the same molecule in solution. This dependence is due to the influence of the local environment on

the electrochemical potentials of the acid, of its conjugate base, and of the protons. In particular, the acidity of a surface-confined molecule is influenced by the polarity of the surface, interfacial electrostatic fields, and the local structure of the solvent. Discussions of various factors that influence interfacial acidity have been presented by Whitesides et al.,⁷ Bain and Whitesides,¹⁶ and Creager and Clark.¹⁵

Quantitative measurement of the acidity of a surface-immobilized species is a challenging analytical problem, requiring methods that are highly specific and sensitive to the composition and properties of the interface. Direct measurement of the surface concentrations of the acid and its conjugate base provides the most straightforward determination of the surface $pK_{1/2}$ (i.e.,

*Author to whom correspondence should be addressed. E-mail: sukenic@mail.biu.ac.il

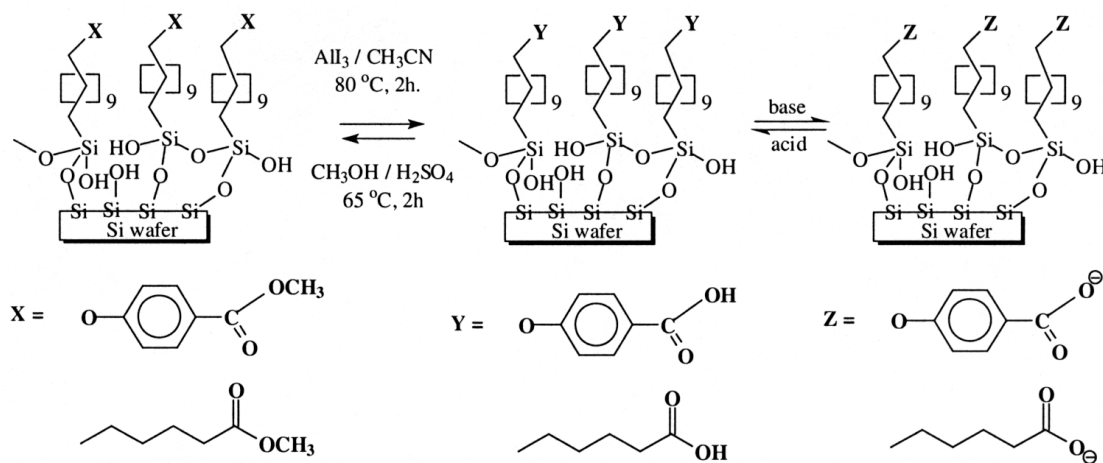
the pH at which half of the surface acid groups are deprotonated, the pK_a). A number of techniques (e.g., contact angle titration,¹⁵⁻¹⁷ quartz microbalance measurements,^{18,19} amperometry,²⁰ voltammetry,^{13,21-23} laser-induced temperature jump studies,²⁴ chemical force microscopy,²⁵⁻²⁸ electrochemical titration,²⁹ double-layer capacitance measurements,³⁰ surface-enhanced Raman spectroscopy³¹) have been applied to determine the pK_a and the double-layer structure of surface-confined acids and bases. Values of the dissociation constants for monolayers carrying carboxylic acid groups vary over a wide range (5.5 to 9.0). The transition from the fully protonated state to the fully dissociated state is also typically much broader than that in the titration of free carboxylic acids in aqueous solution.

Attenuated total reflection Fourier transform infrared spectroscopy (ATR-FTIR) is a technique with sub-monolayer sensitivity that allows the study of the structure and reactivity of molecular adsorbates. In the work reported herein, we explore the properties of carboxylic acids confined to the water/air interface. We use ATR-FTIR spectroscopy to monitor the interconversion between carboxylate esters and acids and to monitor in situ the titration of carboxylic acids (Scheme 1). In situ ATR-FTIR is particularly well suited to measure the pK_a values of carboxylic acid groups confined to the surface, since infrared spectroscopy easily sees the intense bands of the carbonyl of a carboxylic acid and its derivatives and because the carboxylic acid peak and the carboxylate anion peak are well separated and can be observed independently, thus enabling study of the ionization of carboxylic acid groups on the surface.

Experimental data based on changing physical properties is difficult to correlate with structural features at a

molecular level.³²⁻⁴² The acid titration that we report herein addresses this problem by providing molecular information with significantly enhanced sensitivity and resolution. It directly explores the formation of various aggregated forms of carboxylic acid groups on the surface and their influence on the effective pK_a of the array. We demonstrate that hydrogen bonds play a key role in the structure of the acid surface and in conformational changes in the monolayer that can be observed upon deprotonation.

Uniform, siloxane-anchored monolayers terminated with carboxylic acid (COOH) groups cannot be prepared directly because of the chemical incompatibility of the acid functionality with the hydrolyzable silane-anchoring group (e.g., trichlorosilane). Rather, a protected form of the carboxylate must be maintained during monolayer formation. We chose the methyl ester derivative of the alkyl carboxylic acid as a precursor for an acid self-assembled monolayer (SAM) based on its expected ease of hydrolysis and ability to form a well-packed SAM. Unlike more reactive functional groups such as acid chloride,³³ the methyl ester group can survive the process of trichlorosilane anchoring to the surface. Also, the methyl ester is not so big as to interfere with the packing of molecules during the formation of the SAM. De-esterification with a hard Lewis acid (Scheme 1) to a carboxylic acid group is also expected to proceed under mild conditions that should not undermine the siloxane-anchoring network. This is particularly important in light of problems reported with other hydrolysis procedures and the damage they were found to cause.⁴³ The success of AlI_3 in the de-esterification is based on its strength as a Lewis acid and the nucleophilicity of iodide.⁴⁴⁻⁴⁶ The SAM is stable under these



Scheme 1. Schematic of in situ surface de-esterification using ester-bearing siloxane-anchored SAMs.

conditions; i.e., there was no evidence of cleavage of the siloxane-anchoring linkage.⁴³

EXPERIMENTAL: SYNTHESIS OF SURFACTANTS

General: Materials and Analytical Methods

(a) Materials

The following chemicals (>99% pure unless otherwise indicated) were obtained from Aldrich Chemical Company: trichlorosilane (distilled from quinoline immediately prior to use), ω -undecyl alcohol (98%), dicyclohexyl (DCH), hexane (AR), hexane (HPLC), acetone (AR), and hydrogen hexachloroplatinate (IV) hydrate. Methanesulfonyl chloride was obtained from Fluka. CH_2Cl_2 was dried by distillation under N_2 from P_2O_5 . CH_3OH was dried by distillation under N_2 from magnesium turnings. Et_3N was dried by distillation from CaH_2 . THF was dried by distillation under N_2 from Na/benzophenone. Water was deionized and distilled in an all-glass apparatus (DD water).

(b) Equipment and methods

NMR spectra were recorded on a Bruker DPX 300 Spectrometer (units δ , ppm; referenced to TMS for ^1H NMR and to CDCl_3 for ^{13}C NMR) in CDCl_3 solvent. Mass spectra were recorded on a Finnegan model 400, using chemical ionization (CI) with methane as the reagent gas. Distillation conditions are reported as the pot-temperature of the Kugelrohr oven. Column chromatography used silica gel 60 (230–240 mesh) and was done under a positive pressure of nitrogen.

4-Undec-10-enoxybenzoic acid methyl ester (1)

ω -Undecenyl mesylate was prepared as described in ref 47. Into a dry 500-mL flask equipped with a magnetic stirring bar, a reflux condenser, and a drying tube, was placed 300 mL of acetone, ω -undecenyl mesylate (12 g, 48 mmol), potassium carbonate (6.63 g, 48 mmol), and methyl 4-hydroxybenzoate (7.3 g, 48 mmol). The reaction mixture was heated at reflux for 3 days and monitored by TLC (hexane:ethyl acetate 90:10). It was cooled to room temperature and the resulting suspension concentrated on a rotary evaporator. The solid residue was suspended in ether and transferred to a separatory funnel, where it was washed with cold water, 5% NaOH, and saturated aqueous NaCl. It was then dried with MgSO_4 , filtered, and concentrated on a rotary evaporator. The 4-undec-10-enoxybenzoic acid methyl ester (1) was obtained as a clear liquid; purification by chromatography (silica gel; hexane/ethyl acetate 90:10) yielded 6.07 g (42%). ^1H NMR: 6.9 (m, 2H) and 8.0 (m, 2H), 5.8 (m, 1H), 4.7 (m, 2H), 4.01 (t, $J = 5.8$, 2H), 3.8 (s, 3H), 2.04 (m, 2H), 1.75 (m, 2H), 1.45 (m, 12H). ^{13}C NMR: 166.30, 162.38, 139.21, 131.17 (2C), 114.20 (2C), 124.07, 114.50, 68.26, 52.21, 33.82, 29.50 (2C), 29.42, 29.36, 29.18(2C), 26.00. MS: $\text{C}_{19}\text{H}_{28}\text{O}_2$; 304.126 found, 304.14 calcd.

4-(11-Trichlorosilyl-undecyloxy)-benzoic acid methyl ester (2)

Into a 20-mL pressure tube containing a magnetic stirring bar was placed 4-undec-10-enoxybenzoic acid methyl ester (1) (2.38 g, 7.8 mmol), 6 mL of HSiCl_3 , and 10–20 mL of a 4%

solution of $\text{H}_2\text{PtCl}_6 \cdot 6\text{H}_2\text{O}$ in *i*-PrOH. All transfers were done under a nitrogen atmosphere. The progress of the reaction was followed by monitoring the disappearance of olefinic protons in the ^1H NMR. After the reaction was complete, the contents of the tube were transferred (under nitrogen) to a 25-mL round bottom flask. Excess HSiCl_3 was distilled off, and the product was isolated by Kugelrohr distillation at 150 °C (pot temperature) and 0.05 mm Hg, yield 1.12 g, 34%. ^1H NMR: 6.9 (m, 2H) and 8.0 (m, 2H), 4.01 (t, $J = 5.8$, 2H), 3.8 (s, 3H), 1.7 (m, 2H), 1.5 (m, 2H), 1.39 (m, 16H). ^{13}C NMR: 166.30, 162.38, 131.17 (2C), 114.20 (2C), 124.07, 68.26, 52.21, 29.50 (2C), 29.42, 29.36 (2C), 29.18, 29.14, 26.12, 24.43, 22.36.

Methyl 16-heptadecenoate (3)

A flame-dried three-neck 250-mL flask equipped with a pressure-equalizing addition funnel, a reflux condenser with a N_2 inlet, and a magnetic stirring bar, was charged with Mg turnings (4.67 g, 192 mmol). The addition funnel was charged with a solution of 16-bromo-1-hexadecene⁴⁷ (5 g, 16.5 mmol) in 100 mL of dry THF. A portion of this solution (30 mL) was added to the flask to initiate reaction and the rest of the solution was added over a period of 30 min with gentle warming. Completion of Grignard formation required an additional 1 h of reflux (monitored by TLC, silica gel/hexane). The solution was then cooled to room temperature. To another two-neck 250-mL flame-dried flask, fitted with a pressure-equalizing addition funnel, magnetic stirring bar, and N_2 inlet, was added 50 mL of a solution of methyl chloroformate (4 mL, 58 mmol) in THF. This solution was cooled (under nitrogen) in an ice/salt bath to -10 °C. The Grignard reagent from the first flask was transferred to the addition funnel by syringe. It was then added dropwise to the flask. A solution of LiCl (70 mg) and CuCl_2 (200 mg) in THF (15 mL) was then added to the reaction flask. The resulting mixture was stirred at -10 °C for 8 h. Diethyl ether (50 mL) was then added to the flask, and the entire contents were transferred to a separatory funnel. The organic solution was washed twice with saturated aqueous NH_4Cl and once with saturated aqueous NaCl, dried over MgSO_4 , and concentrated on a rotary evaporator. The crude product was purified by flash chromatography (silica gel; hexane/ethyl acetate, 90:10). The yield was 2.48 g, 52%. ^1H NMR: 3.8 (s, 3H), 2.3 (t, $J = 8$, 2H), 5.8 (m, 1H), 4.7 (m, 2H), 1.9–2.1 (m, 2H), 1.6–1.8 (m, 2H), 1.2–1.5 (m, 22H). ^{13}C NMR: 173.9, 138.94, 114.48, 51.53, 34.39, 33.87, 29.60 (2C), 29.31, 29.19 (2C), 28.98 (2C), 28.80 (2C), 28.73 (2C), 25.13. MS: $\text{C}_{18}\text{H}_{34}\text{O}_2$; 282.182 found, 282.17 calcd.

Methyl 17-(trichlorosilyl)heptadecanoate (4)

Into a 20-mL pressure tube containing a magnetic stirring bar was placed methyl 16-heptadecenoate (3) (2.28 g, 8.08 mmol), 7 mL of HSiCl_3 , and 10–20 mL of a 4% solution of $\text{H}_2\text{PtCl}_6 \cdot 6\text{H}_2\text{O}$ in *i*-PrOH. All transfers were done under a nitrogen atmosphere. The progress of the reaction was followed by monitoring the disappearance of olefinic protons in the ^1H NMR. After the reaction was complete, the contents of the tube were transferred (under nitrogen) to a 25-mL round bottom flask. Excess HSiCl_3 was distilled off and the product was isolated by Kugelrohr distillation at 150 °C (pot temperature)

and 0.03 mm Hg to yield a white solid (1.6 g, 47%). ¹H NMR: 3.8 (s, 3H), 2.3 (t, *J* = 8, 2H), 1.6 (m, 4H), 1.2–1.5 (m, 26H). ¹³C NMR: 173.9, 51.53, 34.39, 33.87, 29.60 (2C), 29.31, 29.19 (2C), 28.98, 29.17, 28.80 (2C), 28.73 (2C), 25.13, 24.52, 22.40.

An alternative route to compounds **3** and **4** is reported in ref 48. The material obtained herein was identical, by ¹H NMR, to the material reported therein; for compound (**3**) 1.25 (m, 22H), 1.58–1.64 (m, 2H), 1.99–2.08 (m, 2H), 2.27–2.33 (t, 2H), 3.66 (s, 3H), 4.89–5.02 (m, 2H), 5.73–5.89 (m, 1H); for compound (**4**) 1.25 (m, 26H), 1.56–1.61 (m, 4H), 2.27–2.33 (m, 2H), 3.67 (s, 3H).

Surface Modification with Self-Assembled Monolayers

A. Substrate preparation

For the preparation of SAMs of trichlorosilanes, different substrates were used: n-type silicon wafers (both sides polished) were used for ATR-FTIR (Wafer World Inc., prime grade, <100>, 2–10 Ω·cm, 0.5 μm thickness); and n-type silicon wafers (one side polished) were used for ellipsometry, XPS, and wetting studies (Silicon Sense Inc., prime grade Si, phosphorus-doped <100>, 2–5 Ω·cm, 0.5 μm thickness).

Silicon wafers were cut and then rinsed in chloroform, acetone, and ethanol for 30 s each and dried in a filtered nitrogen stream. Samples were then immersed into piranha solution (concentrated H₂SO₄/H₂O₂ (70:30, v/v)) at 80 °C for 20 min. Samples were then washed 3 times with deionized water and dried in a filtered nitrogen stream. Piranha treatment yielded an oxide layer, which was measured by ellipsometry to be 1.6 ± 0.3 nm thick, and a surface that was totally wetted by water. All the substrates were used within 0.5 h.

B. Deposition of homogeneous (single-component) monolayer films

These wafers were coated with a 0.011 mM solution consisting of 50 μL compound **2** (or **4**) in 10 mL DCH. Deposition times for monolayer formation were typically 1 h for compound (**4**) and 2 h for compound (**2**). After deposition, extensive cleaning of substrates with CH₂Cl₂ (sonication and wiping) was needed.

C. Surface analysis techniques

Contact angle measurements were done on a Rame-Hart Model 100 contact angle goniometer. Measurements were done under ambient conditions. Advancing contact angles were determined by placing a drop (approximate volume 3 μL) of DD water on the sample with a micro-syringe and advancing the volume (adding approximately 2 μL), keeping the area in contact with the substrate constant and leaving the syringe in the drop, and measuring the advancing angle within 30 s of application of the drop. Receding contact angles were determined by withdrawing the water until the lowest angle was achieved without changing the contact area of the drop. Reported values are averages of three measurements taken at difference points on the surface.

ATR-FTIR spectra were measured using a Bruker Vector 22 equipped with an MCT detector. Two-side polished, 500-micron-thick silicon wafers (2 × 5 cm²) were polished on the

cut edges to a 45° angle and used as ATR-IR internal reflection elements. The incident angle (45°) of the infrared beam was controlled to be normal to the bevel surface of the internal reflection element. Prior to collection of the spectra, the sample compartment was purged with nitrogen for 30 min. The spectra (1000 scans) were then acquired using 4 cm⁻¹ resolution and triangular apodization. Each spectrum of coated samples was obtained by subtracting a background obtained using corresponding bare two-sides polished silicon wafer.

Ellipsometric measurements of the thickness of the monolayers were carried out using a variable angle spectroscopic ellipsometer (VASE M-44, from J.A. Woollam Co., polarizer–retarder–sample–rotating analyzer configuration) with a xenon source and a 1-mm spot. Ellipsometric measurements were made after the equipment was calibrated against a 25.0-nm SiO₂ layer on Si. The data were collected at take-off angles of 66°–70° (2° increments) and at 44 fixed wavelengths in the range from 300 to 800 nm (10-nm increments). Prior to each measurement, the optical signal was optimized by focusing the X and Y setting of the light beam. The data were processed using VASE software version 1.1 (J.A. Woollam). The experimental Δ and Ψ data after coating or after in situ surface reaction were fit using a Cauchy model provided by the software to calculate the thickness of the layer, presuming a refractive index of n = 1.45 for this layer. Ellipsometrically determined thickness was compared to a theoretical thickness value estimated from the length of the fully extended chain of the SAM-forming molecule, calculated using PCMODEL (Serena Software). The thickness used for comparison was from the silicon atom of the silane to the most remote atom on the chain.

X-ray photoelectron spectroscopy, XPS, measurements were performed using an AXIS HS (KRATOS ANALYTICAL) X-ray photoelectron spectrometer. The excitation source is a mono Al anode with specific radiation energy of 1486.6 eV. Pass energy for survey and high-resolution scans was 40.0 eV. All binding energies are referenced to C (1s) signal of saturated hydrocarbon at 284.7.0 eV.

In situ Surface Transformation from Ester- to Carboxylic (Benzoic) Acid-Functionalized Monolayers

Carboxylic acid (benzoic acid) monolayers were obtained on a silicon surface by reaction of the methyl ester-bearing surface with AlI₃. This procedure was adapted from the reported procedure for cleaving esters to carboxylic acid in solution.⁴⁹ Ester-functionalized SAM-coated wafers were placed in an oven-dried 150-mL flat-bottom flask, equipped with a small magnetic stirring bar and a reflux condenser, and maintained under a nitrogen atmosphere. To the flask, dry CH₃CN (60 mL) was added. After stirring for 15 min under nitrogen, AlI₃ (0.6 g, 1.47 mmol) was added to the flask. The reaction was heated at reflux (85 °C) for 2 h with vigorous stirring. After cooling the reaction solution to room temperature, the substrate was rinsed with fresh CH₃CN and then with distilled water and placed in 10% HCl for 1 h in order to remove aluminum salts. The resulting modified wafer was then rinsed with water, dried with a stream of nitrogen, and

sonicated in ethanol 10 min. Successful reaction was evidenced by disappearance of the ester carbonyl peak and appearance of an acid carbonyl peak in the IR spectrum. The surface of the modified wafer was characterized by wetting, XPS, and ellipsometry measurements.

In situ Surface Transformation from Carboxylic Acid-to Ester-Functionalized Monolayers

Ester monolayers were obtained on a silicon surface by reacting surface carboxylic acids with methanol using sulfuric acid as a catalyst (as done in solution). Carboxylic acid-functionalized SAMs were placed in a 150-mL flat-bottom flask, equipped with a small magnetic stirring bar and a reflux condenser. To the flask, dry CH_3OH (100 mL) and concentrated H_2SO_4 (1 mL) were added. The reaction was heated at reflux (65 °C) for 2 h with vigorous stirring. After 2 h, the solid substrate was rinsed with distilled water and dried with a stream of nitrogen. Successful reaction was evidenced by disappearance of the acid carbonyl peak and appearance of a new ester carbonyl peak in the IR spectrum. The surface of the modified wafer was characterized by wetting and ellipsometry measurements.

In situ ATR-FTIR Spectroscopy

The FTIR cell (Fig. 1) consists of two Teflon plates machined in the form of an open rectangular cavity with drilled-in orifices, which serve as inlet and outlet for the injection and removal of solutions. These plates are placed on either side of the ATR optical element and pressed against silicone gaskets interposed between each of the plates and ATR element, forming two identical chambers with a total 5 mL volume. Compression of the whole assembly is achieved by means of a custom-designed aluminum frame unit that mounts directly onto the ATR reflection optics attachment. This cell arrangement allows solutions to be exchanged without disturbing the position of any of the optical elements. This strategy makes it possible to record in situ ATR-FTIR spectra as SAM deposition is occurring or, for an already-established SAM, to monitor changes in composition as a function of changes in pH (or reaction with other reagents). Such an approach is essential for obtaining pH difference ATR-FTIR spectra (see below) devoid of substantial solvent peaks and/or interfacial features

other than those attributed to the monolayer itself.

The in situ ATR-FTIR measurements were done on a Bruker Vector 22 spectrometer equipped with a liquid nitrogen-cooled MCT detector. Spectra of the as-deposited films were collected using a $60 \times 20 \times 0.5$ mm Si parallelogram prism, prepared in-house by polishing the two short edges of a freshly cut double-side-polished silicon wafer to a 45° angle. Typically, we collected 500 scans at 4 cm^{-1} nominal spectral resolution.

The sample cell was connected via Viton tubes (5 mm i.d.) to a peristaltic pump (Simon varistaltic power pump, Manostat), which provided a continuous, switchable supply of fresh solution at flow rates of 103 mL/min. D_2O (Aldrich) was used as the bulk solvent instead of H_2O , and the pD value of the D_2O solution was adjusted with either DCl (Acros Organics) or NaOD (0.01 M, prepared by reaction of D_2O with Na). The pD was monitored by an auto titrator (794-basic titrino, Metrohm). In our studies, the ionic strengths of all solutions were between 0.01 and 0.02 M; thus, changes in ionic strength should not be playing a significant role in the observed changes in spectral features.⁵⁰ Single beam spectra were collected from pD = 2.0 to pD = 11.5 (for work done at ambient temperature) and up to pD = 12.5 (for work done at 10 °C), in increments of $\Delta\text{pD} = 0.2 \div 0.5$. In experiments starting from acidic solution, the spectrum at pD = 2.0 was used as the background, and in parallel experiments that started from very basic medium, we used the spectrum at pD = 11.5 as reference and successively decreased the pD of the solution. Before each measurement, the solution with the newly adjusted pD was circulated through the flow cell for 15 min. The intervals of time and the change in the pD of solution between each measurement were adjusted so as to guarantee full equilibration of the system at the new pD. The reservoir solution was constantly stirred and air bubbles were excluded from the entire fluid-handling system.

The general experimental procedure was as follows. A background spectrum was collected with pD = 2.0 or pD = 11.5 solution throughout the system with an acid functionalized SAM-coated sample in place. This background spectrum was subtracted automatically from each sample spectrum that was subsequently collected as the titration proceeded.

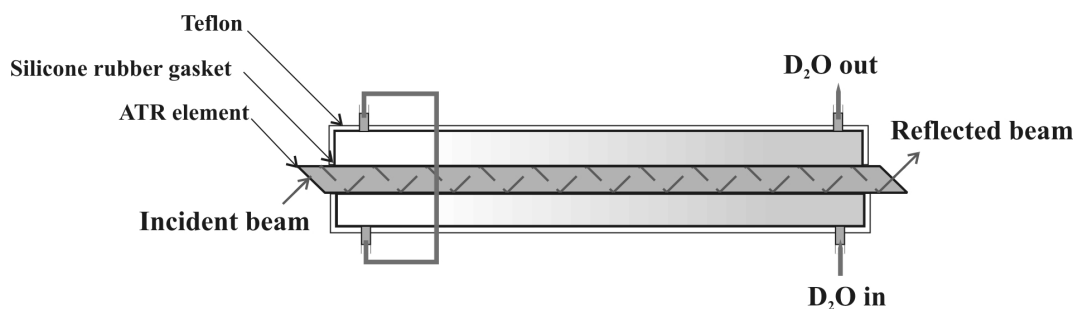


Fig. 1. ATR-FTIR flow-cell construction (top view). The ATR element was clamped between Teflon plates by silicone gaskets. The cavity inside the Teflon holder contains the liquid medium.

Since the humidity in the sample compartment varied, an additional subtraction to correct for varying amounts of water and carbon dioxide was applied. Specifically, an initial background spectrum was recorded and a second background was collected (without changing the sample or the sample compartment in any way). Any difference between these two spectra was due to changes in the moisture level in the sample compartment. This spectrum was used to correct (by proportional subtraction) for additional changes in ambient background conditions.

The procedure employed in this work for the determination of relative surface coverage of the acid/base conjugate species relies on two key points:

- (1) The characteristic IR peaks associated with the RCOOH functional groups, whether protonated acid (1730–1690 cm^{-1}) or deprotonated carboxylate (1540–1590 cm^{-1}), are sufficiently well separated that the overlap is negligible. By using D_2O instead of H_2O we enhance our detection ability in the 1600–1700 cm^{-1} region of the IR spectra. This region is problematic (even with the background subtraction of the difference-spectroscopy method) because of the intense, variable, water signals.
- (2) The effective $\text{p}K_a$ values of the carboxylic (-benzoic) acid-bearing SAMs under study are in the range of 4–10; hence, in strongly acidic and basic media, i.e., $\text{pD} = 2$ and $\text{pD} = 11.5$, the surface functionality is in the fully acidic and fully basic forms, respectively.

Thus, the difference between the single beam spectra of the SAM at a given measured pD and of that same SAM at either of the two extreme pD values should yield positive- and negative-pointing peaks^{33,51} representing the incremental increase and decrease of the acid/carboxylate moieties at the SAM surface at the pD being measured.

RESULTS AND DISCUSSION

The work reported herein first considers the creation of ester-bearing surfaces and their cleavage to provide the acid-bearing surfaces needed for the *in situ* titrations. We then consider the titration experiments done on the acid-bearing SAMs.

The cleavage of the carboxylate ester to form carboxylic acid was monitored by both the changes in the ATR-FTIR spectrum and by the increased hydrophilicity of the surface (Table 1 and Figs. 2 and 3). The spectrum of benzoic acid methyl ester monolayers (Fig. 2) features the carbonyl stretch, $\nu(\text{C}=\text{O})$, as a peak at 1724 cm^{-1} that completely disappeared after reaction with AlI_3 , and a new peak, the $\nu(\text{C}=\text{O})$ of benzoic acid, that appeared at 1685 cm^{-1} (spectrum measured in air). This is similar to the result reported for mercapto-methylterphenylcarboxylic acid on a gold surface.⁵² The acid-stretching frequency corresponds to the value expected for a carboxylic acid dimer.

The peaks at 1606 cm^{-1} and 1512 cm^{-1} are assigned to the aromatic ring. The reduced intensity of the peak at 1606 cm^{-1} is not due to phenyl-ether cleavage (i.e., monolayer degradation) since: (a) the intensity of the second peak of the aromatic ring at 1512 cm^{-1} was not reduced, (b) the thickness of the monolayer (as measured by ellipsometry) after ester cleavage was not reduced, and (c) the XPS shows a comparable signal at 290 eV (corresponding to $\text{C}=\text{O}$), before and after de-esterification. Also, the intensities of methylene peaks at 2922 cm^{-1} and 2852 cm^{-1} before and after reaction are comparable. Table 1 records the results of contact angle, XPS, ellipsometric thickness measurements for methylbenzoate monolayers before and after de-esterification.

Figure 3 shows spectra of the alkyl methyl ester surface before and after treatment with AlI_3 . The peak at 1745 cm^{-1} disappears and a peak at 1714 cm^{-1} (as expected for a carboxylic acid aggregate) is formed. The ester peak can be restored by treatment with methanol and sulfuric acid. The stability of the monolayer to both ester cleavage and ester regeneration (i.e., the reversibility and stability of this system) is in contrast to observations reported for the hydrolysis of ester-terminated alkylsiloxane monolayers with aqueous HCl solution.^{42,43}

The ATR-FTIR spectra of the alkyl carboxylic acid monolayer showed stretching bands $\nu(\text{C}-\text{H})$ at 2920 cm^{-1} and 2851 cm^{-1} . These are slightly shifted relative to the stretching bands $\nu(\text{C}-\text{H})$ for the original methyl ester monolayer (2918 cm^{-1} and 2850 cm^{-1}) in a direction that suggests a somewhat more disordered monolayer surface after the de-esterification reaction. On the other hand, the thickness of the monolayer did not change (Table 1). This change in methylene peak position will be more fully discussed in our analysis of the titration data.

In situ Titration of Acid-Bearing Monolayer Surface Followed by ATR-FTIR

Surface-bound carboxylic acid groups can be inter-converted between protonated and deprotonated forms and then studied by *ex situ* methods. Such studies provide limited information about the pH profile of the ionization of carboxylic acid groups on the surface. Such a profile can only be obtained in a meaningful way by direct monitoring of the titration of the carboxylic acid monolayers. This we do by *in situ* ATR-FTIR. The electrolyte/SAM interface is assumed to be adequately described by a simple two-layer model.⁵³ In this model, all acidic moieties are assumed to lie in the plane of acid dissociation (PAD) at the terminus of the SAM, and the diffuse double layer starts at the PAD and extends into the electrolyte solution. The first layer also includes the entire SAM up to the ionizable functional group.

Table 1. Characterization of methyl ester and acid SAMs by wetting properties, ellipsometry, and XPS

| SAM | contact angle measurements Adv/Rec, ° | thickness, nm | XPS, eV |
|---|--|-----------------|---------|
| $-(\text{CH}_2)_{16}-\text{COOCH}_3$ | $85 \pm 3 / 75 \pm 2$ | 2.26 ± 0.20 | 288.6 |
| $-(\text{CH}_2)_{16}-\text{COOH}$ | $52 \pm 5 / 43 \pm 3$ | 2.31 ± 0.17 | 289.3 |
| $-(\text{CH}_2)_{11}-\text{OC}_6\text{H}_4\text{COOCH}_3$ | $73 \pm 3 / 64 \pm 3$ | 2.0 ± 0.3 | 289.5 |
| $-(\text{CH}_2)_{11}-\text{OC}_6\text{H}_4\text{COOH}$ | $50 \pm 2 / 41 \pm 2$ | 2.2 ± 0.2 | 289.9 |

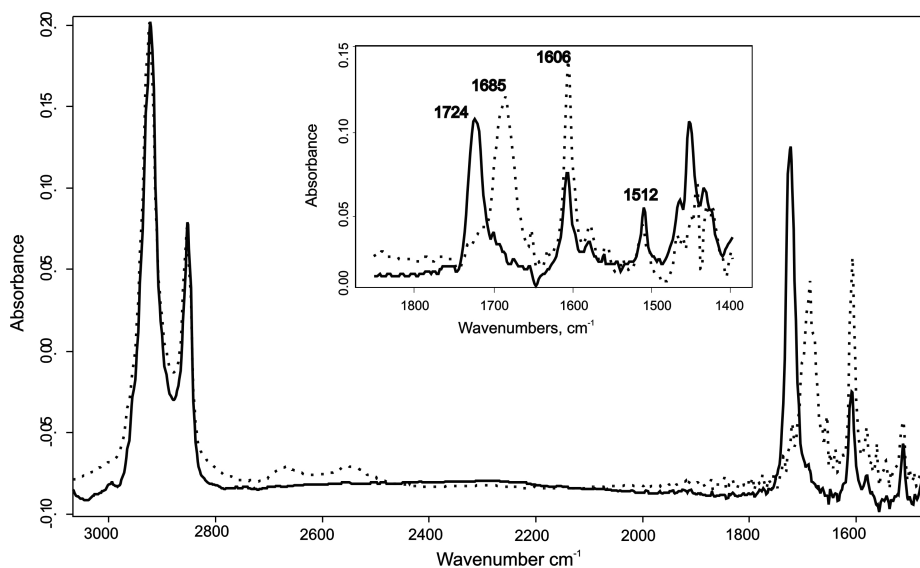


Fig. 2. ATR-FTIR spectra of SAMs on silicon. Solid line is initially deposited methylbenzoate ester SAM (compound 2); dotted line is benzoic acid SAM resulting from de-esterification. Inset: expansion of the carbonyl stretching bands.

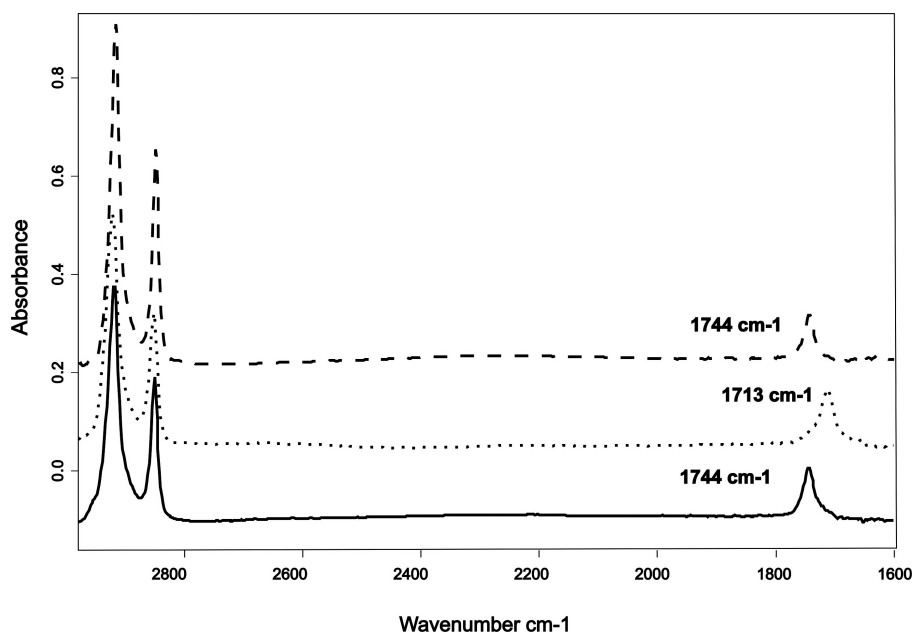


Fig. 3. ATR-FTIR spectra of SAMs. Solid line is initially deposited SAM with terminal methyl ester; dotted line is SAM with terminal carboxylic acid resulting from de-esterification; dashed line is SAM after regenerating the methyl ester.

A. IR assignment of carboxylic and benzoic acids and their salts

The alkyl carboxylic acid, obtained by reaction of methyl ester-SAM with AlI_3 , followed by rinsing in dilute HCl, shows a single peak at 1714 cm^{-1} . This value is observed when the spectrum is measured in air with only surface-adsorbed water. This acid peak is observed at slightly lower frequency ($1702\text{--}1704\text{ cm}^{-1}$) at the D_2O liquid/solid interface. Dipping the sample into aqueous base (0.01 M NaOH) readily transformed the carboxylic acid to its salt, as evidenced by the sharp peak at 1566 cm^{-1} attributable to the carboxylate anion at the air/solid interface.³³ The carboxylic acid groups on the surface are readily regenerated by washing with aqueous HCl (1 M). Here too, the carboxylate anion peak in D_2O solution is observed at slightly lower frequency (1556 cm^{-1}). It evidences pD-dependent changes in shape/position. These have been described^{54–57} as attributable to changes in the relative intensity of split antisymmetric stretching COO^- vibrations at 1542 and 1562 cm^{-1} . Two possible explanations for this splitting are offered in the literature: (1) the band at 1540 cm^{-1} is due to a “hydrated” carboxylate group;⁵⁸ (2) correlated interactions between orientationally nonequivalent molecules.^{54,56}

As expected, the benzoic acid monolayer, obtained by reaction of the ester with AlI_3 , showed peaks at 1685 cm^{-1} and 1606 cm^{-1} , representing the expected carbonyl-stretching frequency and aromatic ring-carbonyl-stretching frequency. These values are observed when the spectrum is measured in air. The stretching frequency of a benzoate salt carbonyl in D_2O solution is observed at 1540 cm^{-1} and that of the aromatic ring of the benzoate salt is at 1592 cm^{-1} . We also see peaks at 2670 cm^{-1} and 2554 cm^{-1} , which are likely due to the OH of the benzoic acid. These peaks are seen in the spectra taken in air, but are not seen when the sample is in aqueous solution.

B. In situ acid/base titration

Having shown that these surface-bound acids reversibly interconvert between protonated and deprotonated forms, we can study their ionization profile under various aqueous (D_2O) buffers. Nevertheless, the use of D_2O instead of H_2O to improve the window of IR transparency raises the question of how such a change might alter our titration results.

The simple ionization process is a special case of a solvent isotope effect. It has long been known that H_2O has a larger self dissociation constant than D_2O , and that dissociation constants of weak acids are larger in H_2O than in D_2O . The isotope effect when substituting deuterium for hydrogen in carboxylic and other acids results

in a ratio $K_{\text{H}} : K_{\text{D}} > 1$. This ratio increases with decreasing acid strength, varying from 1.71 for H_3PO_4 (K_1) to about 6.5 for H_2O . This difference of dissociation constants gives a ready explanation for the greater rate in D_2O (by factors up to 3) in acid-catalyzed reactions in which the rate depends on an equilibrium concentration of the conjugate acid of the reactants. Hepler reported⁵⁹ that internal energy effects, i.e., isotope effects on the O–H or O–D bonds, rather than external effects, such as isotope effects on dielectric constants of solvents or hydrogen bonding between solvent and solute, played the most important role in determining the solvent isotope effect. Nevertheless, the $\text{p}K_{\text{H}}$ of acetic acid is 4.75 and $\text{p}K_{\text{D}}$ is 5.27⁶⁰; $\text{p}K_{\text{H}}$ of benzoic acid is 4.16 and $\text{p}K_{\text{D}}$ is 4.65.⁶⁰ These differences are consistent with the above treatment and, in terms of our experimental data, they are within the experimental error of our measurements.

There are literature reports that consider the relationship between $\text{p}K_{\text{a}}$ and changes in ionic strength.^{24,62} In solutions with ionic strengths $\leq 1.0\text{ M}$, the $\text{p}K_{\text{a}}$ of carboxylic acids is insensitive to ionic strength. For example, at an ionic strength of 0.01 M the $\text{p}K_{\text{a}}$ of CH_3COOH in a NaClO_4 electrolyte solution is 4.68, at 0.10 M it is 4.60, and at 1.0 M it is 4.64.⁵⁰ At ionic strengths $> 1.0\text{ M}$, the $\text{p}K_{\text{a}}$ values of carboxylic acids increase with increasing ionic strength.⁵⁰ In our studies the ionic strengths of all solutions were between 0.01 and 0.02 M, thus, changes in ionic strength should not be an issue.

A series of pD-difference ATR-FTIR spectra obtained at different pD values (Figs. 4A, 5), using the spectrum acquired at pD = 2 as the reference, displays positive- and negative-pointing peaks at 1556 cm^{-1} and at 1704 cm^{-1} that are attributed to the alkylcarboxylate anion and carboxylic acid moieties, respectively. The decrease of the carboxylic acid peak at 1704 cm^{-1} is accompanied by an increase of carboxylate anion at 1556 cm^{-1} ($\text{COO}^-_{\text{asym}}$) as the pD value increases. Such a series of spectra has two important features: (1) the monotonic increase of carboxylate anion peak and decrease of carboxylic acid peak is consistent with the deprotonation of carboxylic acid groups to carboxylate anion groups on the surface as the pD increases; (2) the isosbestic point (in the alkylcarboxylate system) at 1619 cm^{-1} indicates that this transformation is quantitative. When the temperature of the system being titrated was reduced to $10\text{ }^\circ\text{C}$ the isosbestic point shifted to 1632 cm^{-1} .

Similar behavior is found for the surface-bound benzoic acid. The positive- and negative-pointing peaks are at 1540 cm^{-1} and at 1687 cm^{-1} , and the trends observed are the same. With increasing pD the increasingly positive peak at 1540 cm^{-1} reflects the increased concentra-

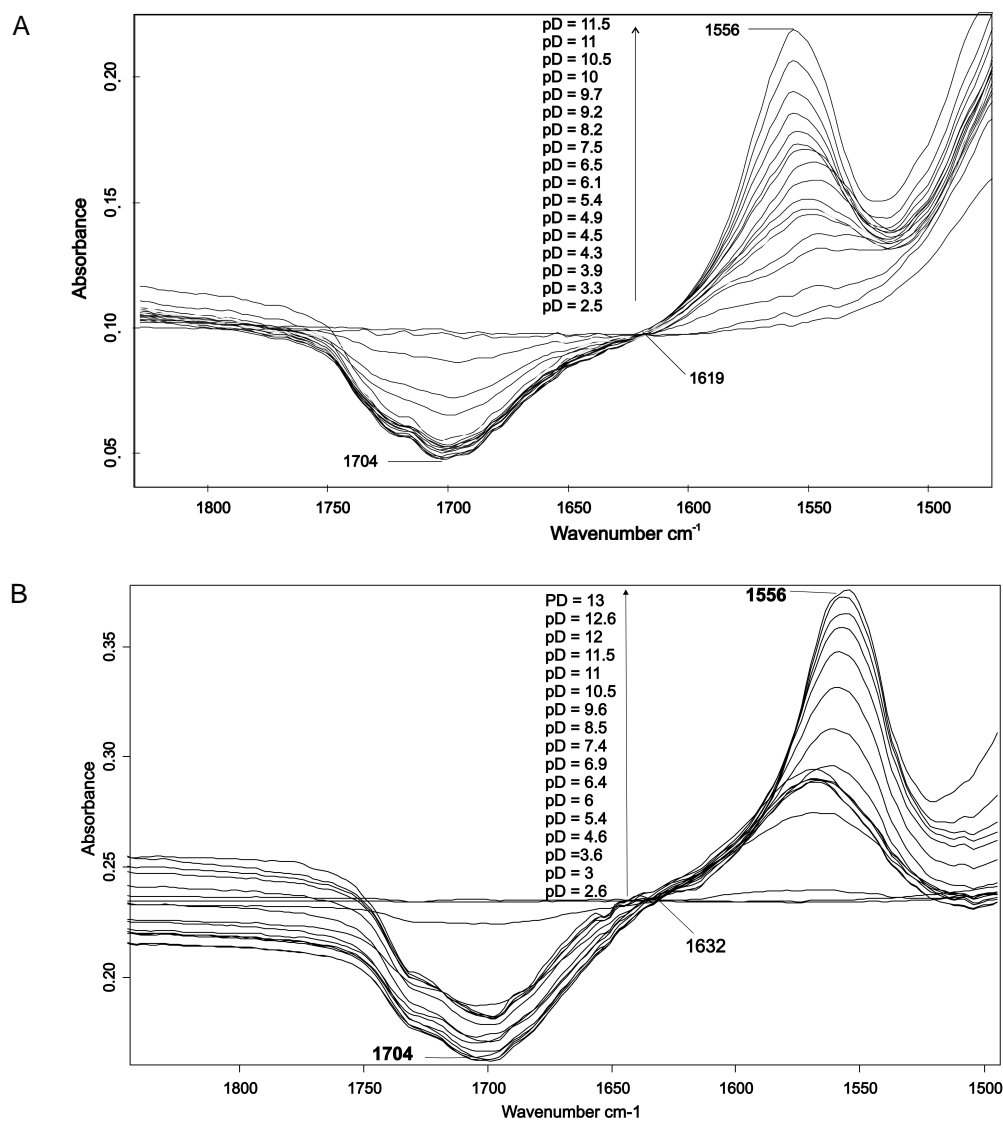


Fig. 4. A representative series of pD-difference ATR-FTIR spectra for a heptadecanoic acid-bearing SAM on Si at (A) r.t.; (B) 10 °C. Spectra were taken while the surface was in contact with solutions of D₂O of various pD. The single-beam spectra of the monolayer in contact with a solution of pD = 2 was used as a reference.

tion of deprotonated benzoate, while an increasingly negative-pointing peak at 1687 cm⁻¹ reflects a decrease in benzoic acid concentration on the surface. Noteworthy is the presence of the peak at 1592 cm⁻¹, attributed to an aromatic ring substituted with a COO⁻. The isosbestic point is at approximately 1630 cm⁻¹.

Using the measured height or the integrated area of the positive peak, it is possible to construct independent plots of each of the two species of interest as a function of pD. Such a plot based on the integrated areas is shown in Fig. 6. For any point in the acid/salt curve, the value on the y axis indicates the ratio of acid to carboxylate groups on the surface and the value on the x axis

indicates the pD value at that point. As indicated in Fig. 6, two pK_a values are observed for both systems: pK_a values of 4.9 ± 0.4 and 9.3 ± 0.2 are obtained for the carboxylic acid, and pK_a values of 4.7 ± 0.3 and 9.0 ± 0.3 for the benzoic acid. When the alkylcarboxylic acid system is cooled to 10 °C, the pK_a values shift to 4.5 ± 0.3 and 10.3 ± 0.3. The existence of two different kinds of deprotonation leads to a broad overall titration profile. The two pK_a values of the monolayer on the surface resemble those reported in bulk solution at high concentration.⁶³ The y-axis values of the plateau observed between the two pK_a values in Fig. 6 represents the percentage of material ionized at the first pK_a. For the

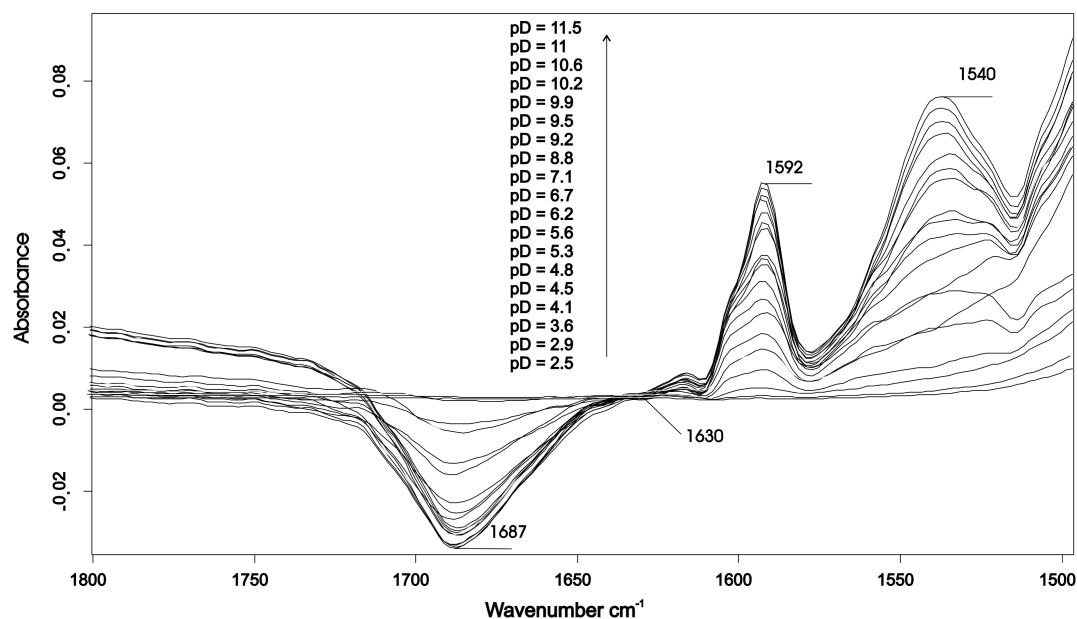


Fig. 5. A representative series of pD-difference ATR-FTIR spectra for a benzoic acid-bearing SAM on Si. Spectra were taken while the surface was in contact with solutions of D₂O of various pD. The single-beam spectra of the monolayer in contact with a solution of pD = 2 was used as a reference.

carboxylic acid this values is ~50% at r.t. and 70% at 10 °C; for the benzoic acid it is ~70%.

When we started the titration from the basic side, we used pD = 11.5 as a reference spectrum. In this case, the pD-difference ATR-FTIR spectra of the alkylcarboxylic acid display positive- and negative-pointing peaks at 1702 cm⁻¹ and at 1560 cm⁻¹, attributed to the carboxylic acid and carboxylate moieties, respectively. The isosbestic point in this case is approximately 1628 cm⁻¹. While the qualitative behavior is the same as when starting from the acid side, it was more difficult to construct similar titration curves since the acid peaks in the subtracted spectra are very broad and the subtraction yields data with less good signal-to-noise ratios.

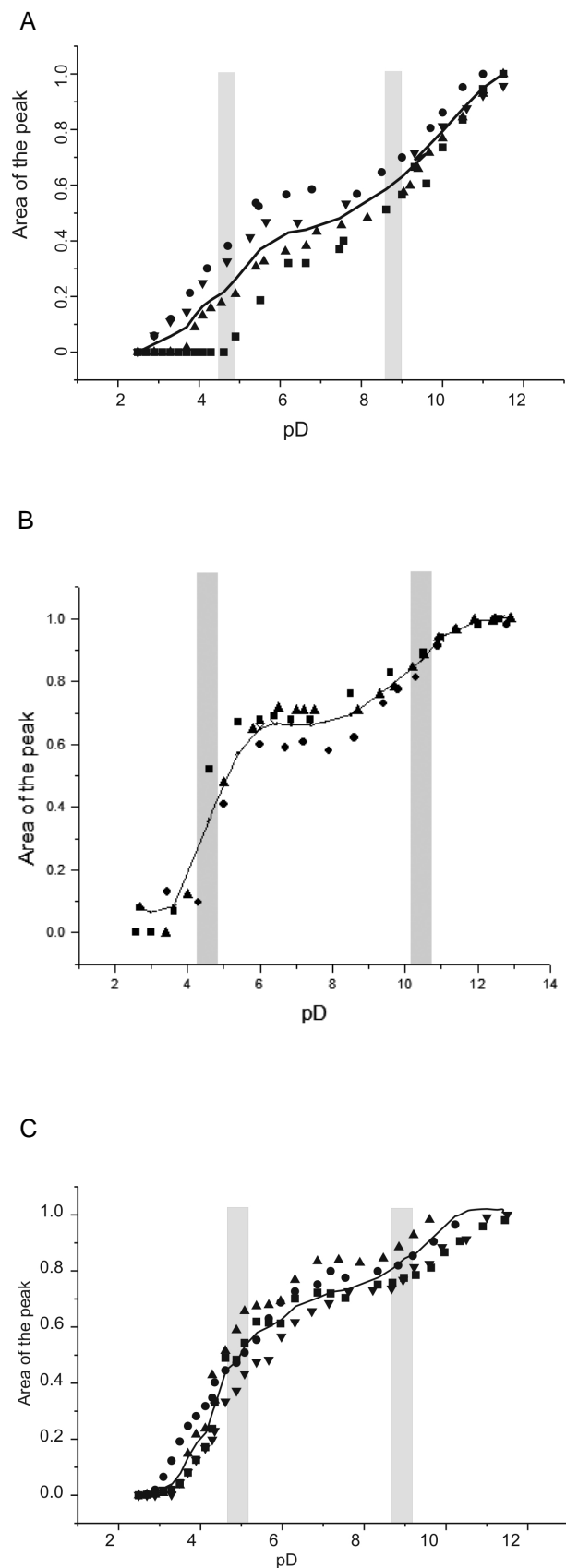
C. Analysis of *in situ* titration

As mentioned previously, the spectral feature observed at 1556 cm⁻¹ is due to the carboxylate anion (COO⁻) group. However, the assignment of the carbonyl peak at 1704 cm⁻¹ is more complex. A deeper understanding of the structural details of the carboxylic acid species was obtained by a careful curve-fitting analysis of the signal from 1760–1610 cm⁻¹. This was only possible for experiments where the reference was pD = 11.5 and the pD was steadily lowered, since only in these experiments are the COOH peaks upward pointing and with sufficient intensity to be candidates for meaningful deconvolution. This set of peaks revealed subtle

changes in shape and position, which we could, by curve fitting, assign to changes in the relative populations of COOH species (COOH that is hydrogen bound only to water, cyclic dimers of COOH, and open-chain oligomers of COOH; Fig. 7). Figure 8 represents the enlarged spectra in the C=O-stretching region at various pD levels. Regrettably, such quantitative analysis is not possible for the benzoate system due to more extensive peak overlap.

We found that three bands, in addition to the water peak at 1645 cm⁻¹, are required to fit the region between 1800 cm⁻¹ and 1600 cm⁻¹ for the pD = 2.2 spectrum. At pD = 2.2 – 5.1, components at 1734, 1703, and 1676 cm⁻¹ are identified. They can be assigned to the C=O-stretching in the monomeric, dimeric, and oligomeric COOH species, respectively. The positions of the free and dimeric C=O bands resemble those previously found for COOH groups in various carboxylic acids.^{64,65} The appearance of a band at 1676 cm⁻¹ has also been reported.^{40,66,67} The oligomer carbonyls have a lower frequency than those of the cyclic dimers because the polarization of the electrons in the oligomeric network of covalent bonds is more extended than in the dimer.⁶⁸

At pD = 6.1, only the carbonyl bands corresponding to the cyclic dimers and the oligomers are seen (Fig. 8, pD = 6.1). The disappearance of the monomeric form (1734 cm⁻¹) signals that the population of different hydrogen-bonded forms changes with pD. By integrating



each of the component peaks at every pD, we can calculate the relative amounts of each of the different kinds of carbonyls and show that the two different bridged species retain a fairly constant ratio of dimer:oligomer of 1.5 ± 0.3 (Table 2). As deprotonation proceeds in progressively more basic solutions, the ratio of aggregated forms cannot be determined since the COOD peaks are too small to be reliably deconvoluted. We also recognize that, lacking relative extinction coefficients for the different forms of COOD, these numbers do not strictly represent the absolute quantitative amount of the various forms. However, their coexistence within the monolayer array and the more rapid disappearance of the COOD monomer are clear.

It is also of interest to note that, in addition to the organization of the monolayer entropically promoting aggregate formation, there are reports⁶⁶ that suggest that carboxylic acid dimers increase in stability with increasing length of the nonpolar part of the acid due to favorable hydrophobic interactions between the hydrocarbon portions. For example, palmitic acid has a reported pK_d of 7.6,⁶⁹ consistent with hydrophobic interactions increasing the K_d value with chain length of the carboxylic acid.⁷⁰ Thus, aggregation, particularly of these organized long-chain acids, is to be expected.

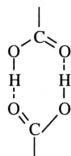
That $50 \pm 10\%$ of the COOD groups deprotonate at $pK_a = 4.9$ (as shown in Fig. 6A), while monomeric COOD accounts for only 20% of the fully protonated COOD groups, can be explained by reference to the dynamic equilibration of the monomer and the aggregates over the course of the titration. We can use the ATR-FTIR delineation of the various forms of the acid group to develop a possible model to more fully describe the acid–base chemistry occurring during our titration experiments. In this model, the first pK involves deprotonation of only the monomeric COOH. We consider the process of deprotonation of the carboxylic acid as occurring in parallel to the equilibration

Fig. 6. pD-titration curves of A—carboxylic acid at r.t.; B—carboxylic acid at 10 °C; C—benzoic acid monolayers on silicon. Each plot contains 4 independent sets of data designated by circles, squares, and triangles up/down. (A) The plot of the amount of carboxylate anion on the surface as a function of pD at r.t. The gray strips indicate the pK_a values (4.9 ± 0.4 and 9.3 ± 0.2) determined by 2nd-derivative analysis of the titration data shown. (B) The plot of the amount of carboxylate anion on the surface as a function of pD at 10 °C. The gray strips indicate the pK_a values (4.5 ± 0.4 and 10.3 ± 0.2) determined by 2nd-derivative analysis of the titration data shown. (C) The plot of the amount of benzoate anion on the surface as a function of pD. The gray strips indicate the pK_a values (4.7 ± 0.3 and 9.0 ± 0.3) determined by 2nd-derivative analysis of the titration data shown.

(a) Free monomer

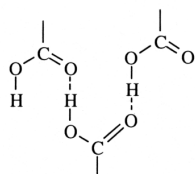


(b) Cyclic dimer



(c) Oligomeric forms

face-on



lateral

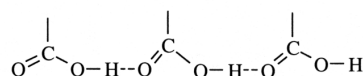
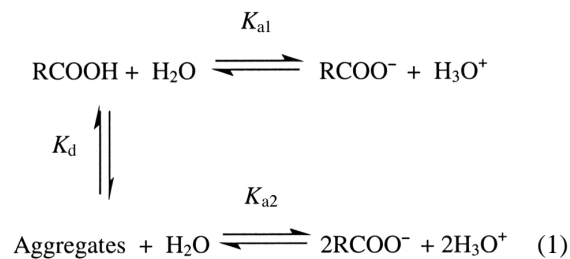


Fig. 7. Structure of (a) free carboxylic acid, (b) and (c) with various arrangements of hydrogen bonds between the carboxylic acid groups.

of the variously aggregated COOH species. Since we cannot separately characterize the chemistry of the dimers and oligomers, we consider them herein under the general heading of “aggregates”.



If we write the expression for the deprotonation equilibrium, we get

$$\text{pD} = \text{p}K_{a1} + \log \frac{[\text{RCOO}^-]}{[\text{RCOOH}]} \quad (2)$$

and

$$\text{pD} = \frac{1}{2} \text{p}K_{a2} + \frac{1}{2} \log \frac{[\text{RCOO}^-]^2}{[\text{Aggregates}]} \quad (3)$$

Fig. 8. Curve-fitting of the C=O-stretching band at various pD values: pD = 2.2, pD = 3.2, pD = 3.8, pD = 4.2, pD = 5.1, pD = 6.1. Dotted lines are the experimental spectra. Solid lines are the resolved components based on the 2nd-derivative method of deconvolution and the fitted sum of the resolved peaks ($R^2 > 0.99$). The position of the three C=O peaks doesn't change in the deconvolution, but the shape of the peaks does vary. The peak at 1645 cm^{-1} is due to water.

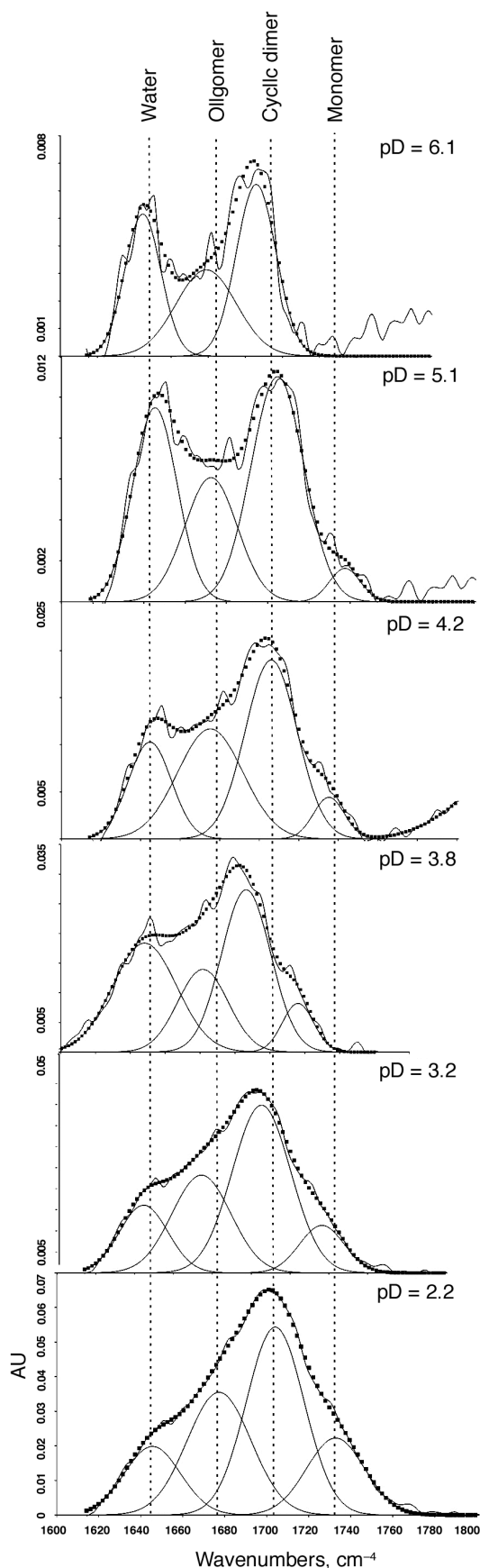


Table 2. Distribution of COOD forms (each deconvolution $R^2 \geq 0.99$)

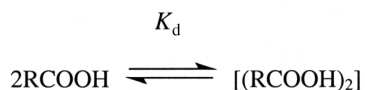
| pD \pm 0.3 | COOD species, % | | |
|--------------|-------------------------------|-------------------------------|-------------------------------|
| | 1734 \pm 3 cm^{-1} | 1703 \pm 3 cm^{-1} | 1676 \pm 2 cm^{-1} |
| 2.2 | 21 \pm 3 | 44 \pm 3 | 35 \pm 1 |
| 2.6 | 17 \pm 2 | 50 \pm 3 | 33 \pm 1 |
| 3.2 | 13 \pm 2 | 54 \pm 3 | 33 \pm 3 |
| 3.8 | 11 \pm 1 | 58 \pm 2 | 31 \pm 1 |
| 4.2 | 7 \pm 0 | 52 \pm 3 | 39 \pm 1 |
| 5.1 | 5 \pm 0 | 59 \pm 2 | 36 \pm 2 |
| 6.1 | 0 | 58 \pm 2 | 42 \pm 2 |

In both eqs 2 and 3, $[\text{RCOOH}]$ is the concentration of the monomer, $[\text{RCOO}^-]$ is the concentration of carboxylate anion, $[\text{Aggregates}]$ is the concentration of cyclic dimer and oligomers, and K_{a1} , K_{a2} are the dissociation constants. Since the total concentration of the self-assembled molecules on the surface, C , is a constant,

$$C = [\text{RCOO}^-] + [\text{RCOOH}] + [\text{Aggregates}] \quad (4)$$

The amount of COO^- species at values of pD < 7 , would be given by eq 2. If $\text{p}K_{a1} = 4.9$, and at pD = 2.2 the concentration of $[\text{RCOOH}]$ is 20% (from experimental data), then the expected concentration of anion at pD = 2.2 would be $[\text{RCOO}^-] = 0.04\%$ (nearly zero). At pD = 6.1, the expected concentration of monomeric acid would be $[\text{RCOOH}] = 4\%$ (too small to measure) and the concentration of carboxylate anion $[\text{RCOO}^-] = 50\%$.

As implied in eq 1, the process of acid aggregation is a separate equilibrium parallel to the deprotonation process. The dimerization constant of the acid (K_d) is the equilibrium of the monomer and dimer:



$$K_d = \frac{[(\text{RCOOH})_2]}{[\text{RCOOH}]^2} \Rightarrow \text{p}K_d = -\log \frac{[(\text{RCOOH})_2]}{[\text{RCOOH}]^2} \quad (5)$$

Since we cannot measure the changes in the ratios of dimer to oligomer as their deprotonation proceeds, we are left to speculate as to the relative ease of their deprotonation. This is a complex issue, since on one hand, the twofold interaction of the pair of hydrogen bonds within the dimer may dominate. On the other hand, it may be that the dimeric COOH groups are ionized more easily than the oligomeric COOH groups. Cyclic dimers of COOH groups require a partial rotation of the carboxylic acid groups about the $\text{C}_\alpha\text{-C}_{=\text{O}}$ bond,

and require significant deviation of the hydrogen bonds from linearity. In such a structure, the energetic cost of the rotation would be compensated for by forming the pair of hydrogen bonds within the dimer. It may be that this barrier is relatively small, as the enthalpy difference between cis-trans isomers of a crystalline long-chain acid is only ~ 0.2 kcal/mol.⁷¹ Therefore, interactions of headgroups with each other and with the solution are likely to be stronger than van der Waals interactions and may dictate the packing within the surface layer. This is a problem that would be interesting to address with FTIR tools of significantly enhanced sensitivity.

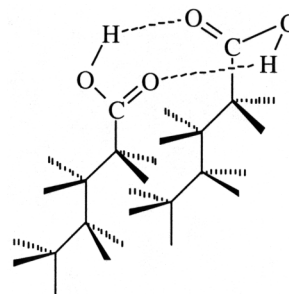


Figure 9 reports changes in the position of the methylene stretches in the IR and allows us to examine structural effects on the SAM alkyl chains that are induced by changes in pD. The position of the $\text{CH}_{2\text{asym}}$ stretch of the alkyl carboxylic acid shifted from 2919 cm^{-1} to 2916 cm^{-1} with increasing pD over the range of 2–7.5. These IR values are comparable to those found for LB layers of long-chain fatty acids compressed to about $22 \text{ \AA}^2/\text{molecule}$ and confirm the close-packed character of the monolayers.⁵⁵ It seems that when approximately half the acid chains are deprotonated (pD = 7 ± 1) they become more rigidly packed, despite the developing anion-anion repulsion. As the pD is made even more basic (up to 11.5), the order is reduced (as evidenced by the $\text{CH}_{2\text{asym}}$ stretch signals in the FTIR going back up to 2920 cm^{-1}). In the experiments done with the alkyl carboxylic acid at 10°C no changes are evident at low pD (< 5), but the trend towards increasing disorder at higher pD is seen clearly (with the $\text{CH}_{2\text{asym}}$ stretch reaching 2923 cm^{-1} at pD 12.53). In the case of benzoic acid, these shifts were less clear and no conclusions could be drawn. Limited attempts to see changes in the structure/packing of the benzoic acid film using AFM were also not successful.

It is interesting to compare these observations to studies in the literature that use grazing incidence X-ray diffraction (GIXD) methods to study the structural diversity of thin films of carboxylic acids at the air/water interface.^{72–75} Datta et al.⁷² use GIXD to consider pH-dependent changes. Consistent with our finding in the high pD region, they show that increasing the pH of the

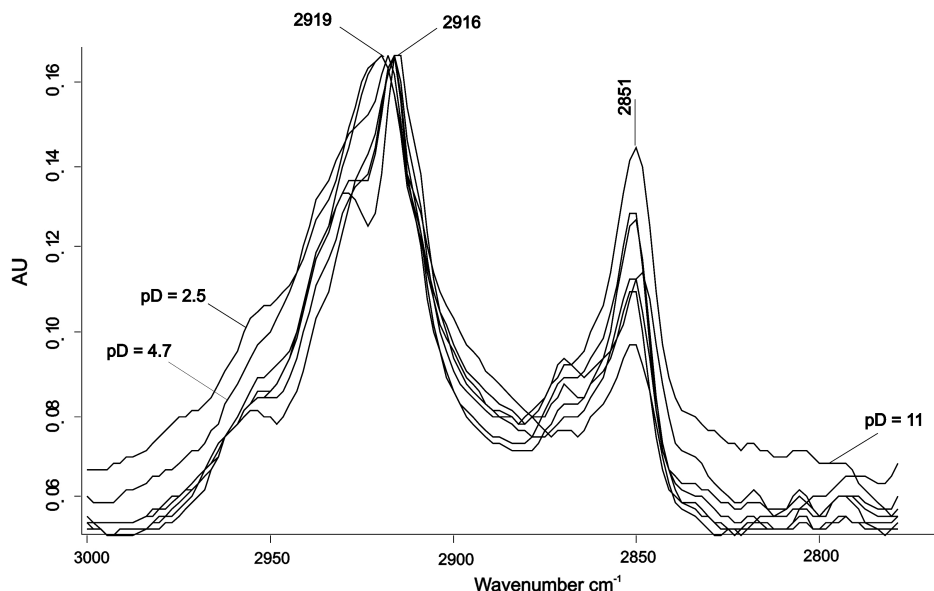


Fig. 9. ATR-FTIR spectra of alkyl carboxylic acid in various pD solutions of D_2O . These spectra demonstrate the different positions of CH_{2sym} and CH_{2asym} vibrations.

monolayer subphase from 10 to 12 results in increasing disorder. They do not report the corresponding data for lower pH values. The picture that emerges of increasing order (presumably due to bridging hydrogen bonds) at low degrees of ionization, giving way to increasing disorder due to charge repulsion at high degrees of deprotonation, is both interesting and consistent with all of the available data.

CONCLUSIONS

We have used ATR-FTIR to study the ionization of surface-bound carboxylic acid groups. We report herein an ATR-FTIR analysis of a carboxylic acid-functionalized siloxane-anchored monolayer that, for the first time, directly measures the balance among differently associated interfacial carboxylic acid groups on the surface and relates their hydrogen bonding with surrounding water molecules and/or among themselves to changes in chain conformation and carboxylate acidity. On the basis of the above experimental results, we conclude that the hydrogen bonds between COOH groups on the surface persist over a pD range of ~ 2.2 – 10.5 . Our results show that a carboxylic acid-bearing SAM is comprised of multiple bridged/unbridged forms at the solid–water interface. Their protonation/deprotonation can be directly monitored. The intermolecular bridging influences SAM structure and chemistry.

We also report the direct observation of 2 different pK_a values within a SAM array, analogous to that which

has been previously reported for a number of aggregates of acids and other constrained situations. The pK_a of micellized fatty acids are reported between 8.6 and 9.7 (similar to our bridged/aggregated transition at 9.3), with crystallization–precipitation occurring at pH 4–5.⁷⁶ Langmuir films of fatty acids show transitions at 3.9 and 10.5.⁷⁷ The geometrically constrained diacid described by Rebek et al.⁷⁸ is also an interesting precedent. Deprotonation of one carboxylic acid influences its intramolecular complexation to the other, and the remaining hydrogen bond is strengthened such that pK_a values of 4.8 and 11.1 are reported.

The model we have used to explain our results incorporates the fact that SAMs terminated with carboxylic acid groups form hydrogen bonds in the plane of the monolayer–water interface. This lateral hydrogen bonding and the molecular packing density makes deprotonation of the surface groups energetically less favorable. At pD = 8, the surface field resulting from the ionization of the monolayer is likely strong enough to reorient both the acid groups and the surrounding water molecules and form ion pairs between the deprotonated acid groups and solution cations. As the pD increases, the monolayer gets more ionized. The monolayer is about half ionized at pD ~ 6 and fully ionized at pD 11.5. The pK_a shift with decreasing of temperature can be explained by reorientation of acid groups or change in conformation of alkyl chain (more crystallinity).

Future directions for this work include an effort to determine the pK_a of mixed monolayers, where the car-

boxylic acid group is diluted within the monolayer surface. The microenvironment of COOH groups in a mixed monolayer is different from that of a pure COOH surface. We will determine the pK_a of mixed monolayers, where the carboxylic acid group is diluted within the monolayer surface, including both hydrophobic and hydrophilic dilution experiments, so as to develop a better understanding of the behavior of this interfacial chemistry. For example, dilution with hydrophobic chains would create a low dielectric microenvironment around the COOH groups that should make it difficult for COOH groups to be deprotonated. On the other hand, the lack of intermolecular hydrogen bonding could lead to a lower pK and make the acid groups easier to deprotonate. Variations in these effects as the diluent is varied between hydrophobic and hydrophilic groups will be most informative. Work in this direction, developing even more sensitive FTIR capabilities so as to allow titration of submonolayer acid concentrations, is underway.

Acknowledgments. Financial support of this work by the Minerva Center for Microscale and Nanoscale Particles and Films as Tailored Biomaterial Interfaces and by the Israel Science Foundation is gratefully acknowledged.

REFERENCES AND NOTES

- (1) Adamson, A.W. *Physical Chemistry of Surfaces*; 4th ed.; Wiley: New York, 1982.
- (2) Andrade, J.D. *Surface and Interfacial Aspects of Biomedical Polymers*; Plenum Press: New York, 1985.
- (3) Grundke, K.; Jacobasch, H.J.; Simon, F.; Schneider, S. *J. Adhes. Sci. Technol.* **1995**, *9*, 9327–9350.
- (4) Hunter, R.J. *Foundations of Colloid Sciences*; Clarendon Press: London, 1986.
- (5) Lyklema, J. *Fundamentals of Interface and Colloid Science*; Academic Press: London, 1995; Vol. 1 and 2.
- (6) van Oss, C.J.; Chaudhury, M.K.; Good, R. *J. Chem. Rev.* **1988**, *88*, 927.
- (7) Whitesides, G.M.; Biebuyck, H.A.; Folkers, J.P.; Prime, K.L. *J. Adhes. Sci. Technol.* **1991**, *5*, 57–69.
- (8) Israelachvili, J. *Intermolecular and Surfaces Forces*; 2nd ed.; Academic Press: London, 1992.
- (9) Li, T. T.-T.; Weaver, M.J. *J. Am. Chem. Soc.* **1984**, *106*, 6107–6108.
- (10) Malem, F.; Mandler, D. *Anal. Chem.* **1993**, *65*, 37–41.
- (11) Sun, L.; Crooks, R.M.; Ricco, A.J. *Langmuir* **1993**, *9*, 1775–1780.
- (12) Turyan, I.; Mandler, D. *Anal. Chem.* **1994**, *66*, 58–63.
- (13) Bryant, M.A.; Crooks, R.M. *Langmuir* **1993**, *9*, 385–387.
- (14) Sun, L.; Johnson, B.; Wade, T.; Crooks, R.M. *J. Phys. Chem.* **1990**, *94*, 8869–8871.
- (15) Creager, S.E.; Clarke, J. *Langmuir* **1994**, *10*, 3675–3683.
- (16) Bain, C.D.; Whitesides, G. M. *Langmuir* **1989**, *5*, 1370–1378.
- (17) Lee, T.R.; Carey, R.I.; Biebuyck, H.A.; Whitesides, G.M. *Langmuir* **1994**, *10*, 741–749.
- (18) Shimazu, K.; Teranishi, T.; Sugihara, K.; Uosaki, K. *Chem. Lett.* **1998**, 669–670.
- (19) Wang, J.; Frostman, L.M.; Ward, M.D. *J. Phys. Chem.* **1992**, *96*, 5224–5228.
- (20) Cheng, Q.; Braithier-Toth, A. *Anal. Chem.* **1992**, *64*, 1998–2000.
- (21) Godinez, L.A.; Castro, R.; Kaifer, A. E. *Langmuir* **1996**, *12*, 5087–5092.
- (22) White, H.S.; Peterson, J.D.; Cui, Q.Z.; Stevenson, K.J. *J. Phys. Chem. B* **1998**, *102*, 2930–2934.
- (23) Molinero, V.; Calvo, E.J. *J. Electroanal. Chem.* **1998**, *445*, 17–25.
- (24) Smalley, J.F.; Chalfant, K.; Feldberg, S.W.; Nahir, T.M.; Bowden, E.F. *J. Phys. Chem. B* **1999**, *103*, 1676–1685.
- (25) He, H.X.; Huang, W.; Zhang, H.; Li, Q.G.; Li, S.F.Y.; Liu, Z.F. *Langmuir* **2000**, *16*, 517–521.
- (26) Hu, K.; Bard, A.J. *Langmuir* **1997**, *13*, 5114–5119.
- (27) Kokkoli, E.; Zukoski, C.F. *Langmuir* **2000**, *16*, 6029–6036.
- (28) Kane, V.; Mulvaney, P. *Langmuir* **1998**, *14*, 3303–3311.
- (29) Zhao, J.; Luo, L.; Yang, X.; Wang, E.; Dong, S. *Electroanalysis* **1999**, *11*, 1108.
- (30) Kakiuchi, T.; Iida, M.; Imabayashi, S.; Niki, K. *Langmuir* **2000**, *16*, 5397–5401.
- (31) Mullen, K.I.; Wang, D.X.; Crane, L.G.; Carron, K.T. *Anal. Chem.* **1992**, *64*, 930–936.
- (32) Dannenberger, O.; Weiss, K.; Himmel, H.-J.; Jager, B.; Buck, M.; Woll, C. *Thin Solid Films* **1997**, *307*, 183–191.
- (33) Cheng, S.S.; Scherson, D.A.; Sukenik, C.N. *Langmuir* **1995**, *11*, 1190–1195.
- (34) Holmes-Farley, S.R.; Reamey, R.H.; McCarthy, T.J.; Deutch, J.; Whitesides, G.M. *Langmuir* **1985**, *1*, 725–740.
- (35) Holmes-Farley, S.R.; Whitesides, G.M. *Langmuir* **1987**, *3*, 62–76.
- (36) Holmes-Farley, S.R.; Bain, C.D.; Whitesides, G.M. *Langmuir* **1988**, *4*, 921–937.
- (37) Ferguson, G.S.; Chaudhury, M.K.; Biebuyck, H.A.; Whitesides, G.M. *Macromolecules* **1993**, *26*, 5870–5875.
- (38) Balachander, N.; Sukenik, C.N. *Langmuir* **1990**, *6*, 1621–1627.
- (39) Nuzzo, R.G.; Dubois, L.H.; Allara, D.A. *J. Am. Chem. Soc.* **1990**, *112*, 558–569.
- (40) Smith, E.L.; Alves, C.A.; Anderegg, J.W.; Porter, M.D.; Siperko, L.M. *Langmuir* **1992**, *8*, 2707–2714.
- (41) Taylor, M.D.; Bruton, J. *J. Am. Chem. Soc.* **1952**, *74*, 4151–4152.
- (42) Wasserman, S.R.; Tao, Y.-T.; Whitesides, G.M. *Langmuir* **1989**, *5*, 1074–1087.
- (43) Fryxell, G.E.; Rieke, P.C.; Wood, L.L.; Engelhard, M.H.; Williford, R.E.; Graff, G.L.; Campbell, A.A.; Wiacek, R.J.; Lee, L.; Halverson, A. *Langmuir* **1996**, *12*, 5064–5075.
- (44) Mahajan, A.R.; Dutta, D.K.; Boruah, R.C.; Sandhu, J.S. *Tetrahedron Lett.* **1990**, *27*, 3943–3944.

- (45) Mc Murry, J.E. *Org. Reactions* **1976**, *24*, 187.
- (46) Nagata, W.; Wakabayashi, T.; Narisada, M.; Hayase, Y.; Kumata, S. *J. Am. Chem. Soc.* **1971**, *93*, 5740–5758.
- (47) Balachander, N.; Sukenik, C.N. *Langmuir* **1990**, *6*, 1621–1627.
- (48) Vallant, T.; Kattner, J.; Brunner, H.; Mayer, U.; Hoffmann, H. *Langmuir* **1999**, *15*, 5339–5346.
- (49) Mahajan, A.R.; Dutta, P.K.; Boruah, R.C.; Sandhu, J.S. *Tetrahedron Lett.* **1990**, *31*, 3943–3944.
- (50) Rossotti, F.J.; Rossotti, H. *The Determination of Stability Constants and Other Equilibrium Constants in Solution*; McGraw-Hill: New York, 1962.
- (51) Chang, S.C.; Weaver, M.J. *J. Phys. Chem.* **1991**, *95*, 5391.
- (52) Arnold, R.; Azzam, W.; Terfort, A.; Woll, C. *Langmuir* **2002**, *18*, 3980–3992.
- (53) Delahay, P. *Double Layer and Electrode Kinetics*; Wiley: New York, 1965.
- (54) Jakupca, M.; Dutta, P.K. *Chem. Mater.* **1995**, *7*, 989.
- (55) Gericke, A.; Huhnerfuss, H. *J. Phys. Chem.* **1993**, *97*, 12899–12908.
- (56) Borja, M.; Dutta, P.K. *J. Phys. Chem.* **1992**, *96*, 5434–5444.
- (57) Wong, P.T.T.; Mantsch, H.H. *J. Colloid Interface Sci.* **1989**, *129*, 258.
- (58) Dreamer, D.W.; Meek, D.W.; Cornwell, D.G. *J. Lipid. Res.* **1967**, *8*, 255.
- (59) Hepler, L.G. *J. Phys. Chem.* **1964**, *68*, 2645.
- (60) La Mer, V.K.; Korman, S. *Science* **1936**, *83*, 624.
- (61) Wehry, E.L.; Rogers, L.B. *J. Am. Chem. Soc.* **1966**, *88*(2), 351.
- (62) Smith, E.L.; Wallwork, M.L.; Zhang, J.; Kirkham, J.; Robinson, C.; Marsh, A.; Wong, M. *J. Phys. Chem. B* **2000**, *104*, 8862–8870.
- (63) Schrier, E.E.; Pottle, M.; Scheraga, H.A. *J. Am. Chem. Soc.* **1964**, *86*, 3444.
- (64) Dubin, P.L.; Strauss, U.P. *J. Phys. Chem.* **1970**, *74*, 2842.
- (65) Dong, J.; Tsubahara, N.; Fujimoto, Y.; Ozaki, Y.; Nakashima, K. *Appl. Spectrosc.* **2001**, *55*, 1603–1609.
- (66) Tanaka, N.; Kitano, H.; Ise, N. *J. Phys. Chem.* **1990**, *94*, 6290–6292.
- (67) Genin, F.; Quiles, F.; Burneau, A. *Phys. Chem. Chem. Phys.* **2001**, *3*, 932–942.
- (68) Dong, J.; Ozaki, Y.; Nakashima, K. *Macromolecules* **1997**, *30*, 1111.
- (69) Eagland, D.; Franks, F. *Trans. Faraday Soc.* **1965**, *61*, 2468.
- (70) Tanaka, N.; Kitano, H.; Ise, N. *J. Phys. Chem.* **1991**, *95*, 1503–1507.
- (71) Hayashi, S.; Umemura, J. *J. Chem. Phys.* **1975**, *63*, 1732–1744.
- (72) Datta, A.; Kmetko, J.; Richter, A. G.; Yu, H.-Z.; Dutta, P.K.; Chung, K.-S.; Bai, J.-M. *Langmuir* **2000**, *16*(3), 1239–1242.
- (73) Weissbuch, I.; Berkovic, G.; Yam, R.; Als-Nielsen, J.; Kjaer, K.; Lahav, M.; Leiserowitz, L. *J. Phys. Chem.* **1995**, *99*(16), 6036–6045.
- (74) Boehm, C.; Leveiller, F.; Jacquemain, D.; Moehwald, H.; Kjaer, K.; Als-Nielsen, J.; Weissbuch, I.; Leiserowitz, L. *Langmuir* **1994**, *10*(3), 830–836.
- (75) Rapaport, H.; Kuzmenko, I.; Berfeld, M.; Kjaer, K.; Als-Nielsen, J.; Popovitz-Biro, R.; Weissbuch, I.; Lahav, M.; Leiserowitz, L. *J. Phys. Chem. B* **2000**, *104*(7), 1399–1428.
- (76) Kanicky, J.R.; Shah, D. *J. Colloid Interface Sci.* **2002**, *256*, 201–207.
- (77) Miranda, P.B.; Du, Q.; Shen, Y.R. *Chem. Phys. Lett.* **1998**, *286*, 1–8.
- (78) Rebek, J.Jr.; Duff, R.J.; Gordon, W.E.; Parris, K. *J. Am. Chem. Soc.* **1986**, *108*, 6068–6069.